

## Preliminary Design of LUCID

### The Lunar Unidentified Celestial Identification & Detection Satellite

Acedo, Sergio L.; Pinto, Lucas Adloff Cardoso; Aliaga, Sergi; Baclet, Damien; Baptista, Raquel; Betco, Daniel; Bischof, Reto; Michahelles, Margherita; Yadav, Sachin; Janisch, K.I.

**DOI**

[10.52202/078365-0132](https://doi.org/10.52202/078365-0132)

**Publication date**

2024

**Document Version**

Final published version

**Published in**

IAF Space Systems Symposium - Held at the 75th International Astronautical Congress, IAC 2024

**Citation (APA)**

Acedo, S. L., Pinto, L. A. C., Aliaga, S., Baclet, D., Baptista, R., Betco, D., Bischof, R., Michahelles, M., Yadav, S., Janisch, K. I., & More Authors (2024). Preliminary Design of LUCID: The Lunar Unidentified Celestial Identification & Detection Satellite. In *IAF Space Systems Symposium - Held at the 75th International Astronautical Congress, IAC 2024* (pp. 1188-1204). (Proceedings of the International Astronautical Congress, IAC; Vol. 2-B). International Astronautical Federation, IAF. <https://doi.org/10.52202/078365-0132>

**Important note**

To cite this publication, please use the final published version (if applicable).  
Please check the document version above.

**Copyright**

Other than for strictly personal use, it is not permitted to download, forward or distribute the text or part of it, without the consent of the author(s) and/or copyright holder(s), unless the work is under an open content license such as Creative Commons.

**Takedown policy**

Please contact us and provide details if you believe this document breaches copyrights.  
We will remove access to the work immediately and investigate your claim.

***Green Open Access added to TU Delft Institutional Repository***

***'You share, we take care!' - Taverne project***

**<https://www.openaccess.nl/en/you-share-we-take-care>**

Otherwise as indicated in the copyright section: the publisher is the copyright holder of this work and the author uses the Dutch legislation to make this work public.

IAC-24-B4-IP-31-x83861

## Preliminary Design of LUCID: The Lunar Unidentified Celestial Identification & Detection Satellite

**Sergio López Acedo<sup>1</sup>, Lucas Adloff Cardoso Pinto<sup>2</sup>, Sergi Aliaga<sup>3</sup>, Damien Baclet<sup>4</sup>, Raquel Baptista<sup>5</sup>, Daniel Betco<sup>6</sup>, Reto Bischof<sup>7</sup>, Emanuele Celardo<sup>8</sup>, Angela Cratere<sup>9</sup>, Kamil Dylewicz<sup>10</sup>, Caner Eriş<sup>11</sup>, Sílvia Farràs Aloy<sup>12</sup>, Ross Findlay<sup>13</sup>, Damian Grabowski<sup>14</sup>, Jennifer Hoffmann<sup>15</sup>, Katharina-Inés Janisch<sup>16\*</sup>, Sinan Felix Klein<sup>17</sup>, Wilhelm Kristiansen<sup>18</sup>, Erikas Kymantas<sup>19</sup>, Fabiola Luna La Fazia<sup>20</sup>, Uxía García Luis<sup>21</sup>, Duncan Lyster<sup>22</sup>, Jakub Mašek<sup>23</sup>, Alessandro Mastropietro<sup>24</sup>, Alessandro Miceli<sup>25</sup>, Margherita Michahelles<sup>26</sup>, Nick Parak<sup>27</sup>, Dominika Pytlak<sup>28</sup>, Thorvi Ramteke<sup>29</sup>, Nuno Rebolo<sup>30</sup>, Kristina Remić<sup>31</sup>, Flavie Aditya Annick Suzanne Davida Tohotaua Rometsch<sup>32</sup>, Noah Isaac Sadaka<sup>33</sup>, Christina Sakellari<sup>34</sup>, Daniel Wischert<sup>35</sup>, Sachin Yadav<sup>36</sup>**

<sup>1</sup> *Technical University of Madrid (UPM), Spain, [sergio.lopez.acedo@alumnos.upm.es](mailto:sergio.lopez.acedo@alumnos.upm.es)*

<sup>2</sup> *TU Darmstadt, Germany, [lucas.adloff@stud.tu-darmstadt.de](mailto:lucas.adloff@stud.tu-darmstadt.de)*

<sup>3</sup> *Northeastern University, United States, [aliaga.s@northeastern.edu](mailto:aliaga.s@northeastern.edu)*

<sup>4</sup> *ISAE-Supaero University of Toulouse, France, [damien.baclet@sciencespo.fr](mailto:damien.baclet@sciencespo.fr)*

<sup>5</sup> *Universidade do Minho, Portugal, [raquelbaptista@outlook.pt](mailto:raquelbaptista@outlook.pt)*

<sup>6</sup> *Politehnica University of Bucharest, Romania, [daniel.betco.o@gmail.com](mailto:daniel.betco.o@gmail.com)*

<sup>7</sup> *Lucerne University of Applied Sciences and Arts (HSLU), Switzerland, [r.bischof95@gmail.com](mailto:r.bischof95@gmail.com)*

<sup>8</sup> *University of Warwick, United Kingdom, [emanuele1502celardo@icloud.com](mailto:emanuele1502celardo@icloud.com)*

<sup>9</sup> *Politecnico di Bari, Italy, [a.cratere@phd.poliba.it](mailto:a.cratere@phd.poliba.it)*

<sup>10</sup> *University of Liverpool, United Kingdom, [sgkdylew@liverpool.ac.uk](mailto:sgkdylew@liverpool.ac.uk)*

<sup>11</sup> *TU Darmstadt, Germany, [caner.eris@stud.tu-darmstadt.de](mailto:caner.eris@stud.tu-darmstadt.de)*

<sup>12</sup> *International Space University (ISU), France, [silvia.farras@community.isunet.edu](mailto:silvia.farras@community.isunet.edu)*

<sup>13</sup> *ESA, The Netherlands, [ross.findlay@esa.int](mailto:ross.findlay@esa.int)*

<sup>14</sup> *Lukasiewicz Research Network – Institute of Aviation (ILOT), Poland, [damian.grabowski@ilot.lukasiewicz.gov.pl](mailto:damian.grabowski@ilot.lukasiewicz.gov.pl)*

<sup>15</sup> *TU Darmstadt, Germany, [hoffmann@fsr.tu-darmstadt.de](mailto:hoffmann@fsr.tu-darmstadt.de)*

<sup>16</sup> *Technical University Delft, Faculty of Aerospace Engineering, The Netherlands, [k.i.janisch@student.tudelft.nl](mailto:k.i.janisch@student.tudelft.nl)*

<sup>17</sup> *University Stuttgart, Germany, [st165934@stud.uni-stuttgart.de](mailto:st165934@stud.uni-stuttgart.de)*

<sup>18</sup> *NTNU Trondheim, Norway, [wilhelmkr@gmail.com](mailto:wilhelmkr@gmail.com)*

<sup>19</sup> *Imperial College London, United Kingdom, [erikaskymantas@gmail.com](mailto:erikaskymantas@gmail.com)*

<sup>20</sup> *University of Naples "Federico II", Italy, [luna2001@live.it](mailto:luna2001@live.it)*

<sup>21</sup> *University of Vigo, Spain, [uxia.garcia.luis@uvigo.es](mailto:uxia.garcia.luis@uvigo.es)*

<sup>22</sup> *University of Oxford, United Kingdom, [duncan.lyster@physics.ox.ac.uk](mailto:duncan.lyster@physics.ox.ac.uk)*

<sup>23</sup> *Brno University of Technology, Czech Republic, [Jakub.Masek@vutbr.cz](mailto:Jakub.Masek@vutbr.cz)*

<sup>24</sup> *NanoAvionika UAB (NanoAvionics LLC), Lithuania, [alessandro.mastropietro@nanoavionics.com](mailto:alessandro.mastropietro@nanoavionics.com)*

<sup>25</sup> *Politecnico di Milano, Italy, [alessandro.miceli@mail.polimi.it](mailto:alessandro.miceli@mail.polimi.it)*

<sup>26</sup> *Politecnico di Torino, Italy, [margherita.michahelles@studenti.polito.it](mailto:margherita.michahelles@studenti.polito.it)*

<sup>27</sup> *Vienna University of Technology, Austria, [e12016319@student.tuwien.ac.at](mailto:e12016319@student.tuwien.ac.at)*

<sup>28</sup> *Warsaw University of Technology (WUT), Poland, [dominika.pytlak.stud@pw.edu.pl](mailto:dominika.pytlak.stud@pw.edu.pl)*

<sup>29</sup> *TU Darmstadt, Germany, [thorvi.ramteke@stud.tu-darmstadt.de](mailto:thorvi.ramteke@stud.tu-darmstadt.de)*

<sup>30</sup> *Faculdade de Ciências e Tecnologia - UNL, Portugal, [n.rebolo@campus.fct.unl.pt](mailto:n.rebolo@campus.fct.unl.pt)*

<sup>31</sup> *TU Darmstadt, Germany, [kristina.remic@stud.tu-darmstadt.de](mailto:kristina.remic@stud.tu-darmstadt.de)*

<sup>32</sup> *ESA-ESTEC, The Netherlands, [flavie.rometsch@esa.int](mailto:flavie.rometsch@esa.int)*

<sup>33</sup> *Purdue University, United States, [nsadaka@purdue.edu](mailto:nsadaka@purdue.edu)*

<sup>34</sup> *Aristotle University of Thessaloniki, Greece, [christisakellari@gmail.com](mailto:christisakellari@gmail.com)*

<sup>35</sup> *ESA, The Netherlands, [daniel.wischert@esa.int](mailto:daniel.wischert@esa.int)*

<sup>36</sup> *Delft University of Technology (TU Delft), The Netherlands, [s.yadav-1@tudelft.nl](mailto:s.yadav-1@tudelft.nl)*

\*Corresponding author

## Abstract

This work outlines the Phase 0 design of the Lunar Unidentified Celestial Identification & Detection (LUCID) mission, a sub 200 kg micro-spacecraft developed to observe and track objects larger than 3 metres in diameter at the average distance of the lunar orbit. The mission, planned for launch on a Vega-C rocket into a Sun-synchronous orbit at 500 km, aims to enhance space situational awareness in the cislunar region. The spacecraft's optical payload will survey a defined area at least once daily, contributing to the tracking of space debris as space exploration and cislunar activities expand. The LUCID mission concept was developed by 40 students over one week during the 2023 European Space Agency (ESA) Academy Concurrent Engineering Workshop (CEW), using the COMET tool to achieve a concurrent design of both the space and ground segments. This paper details the preliminary design outcomes and subsystem analyses of the LUCID mission.

**Keywords:** Lunar Orbit, Space Debris Tracking, Space Situational Awareness, Concurrent Engineering, Micro-spacecraft Design, Optical Detection Systems

## Acronyms

AIV	Assembly, Integration, and Verification	S/C	spacecraft
AOCS	Attitude and Orbital Control	SBOC	Space-Based Optical Component
AoI	Area of Interest	SD	Secure Digital
C&DH	Communication and Data Handling	SDRAM	Synchronous Dynamic Random Access Memory
CDF	Concurrent Design Facility	SSD	Solid-State Drive
CEW	Concurrent Engineering Workshop	SSO	Sun Synchronous Orbit
COC	Cold Operational Conditions	TID	Total Ionising Dose
CONOPS	Concept of Operations	TRL	Technology readiness level
COTS	Commercial Off-The-Shelf	TT&C	Telemetry, Tracking and Control
CPU	Central Processing Unit		
DC	Direct Current		
EoL	End of Life		
ESA	European Space Agency		
ESEC	European Space Security and Education Centre		
FDIR	Fault Detection, Isolation and Recovery		
FPGA	Field Programmable Gate Array		
GEO	Geostationary Orbit		
GS	Ground Station		
HOC	Hot Operational Conditions		
ITU	International Telecommunication Union		
L1	Lagrange Point 1 of the Earth-Moon system		
LEO	Low Earth Orbit		
LEOP	Launch and Early Operations Phase		
LUCID	Lunar Unidentified Celestial Identification & Detection		
MLI	Multi-Layer Insulation		
OBC	On-Board Computer		

## 1. Introduction

With an ever-increasing interest in space exploration and plans of permanent human settlements on the Moon, addressing the problem of tracking and removal of space debris has become a major challenge that space-related institutions and companies have to face. According to the ESA Annual Space Environment Report from 2023 [1], the number of launch events is expected to increase as well as the number of total satellites. This rapid increase in objects requires more robust space traffic management practices to prevent collisions and allow spacecraft to operate safely. Similar developments are expected for the cislunar environment, where many programs, like Artemis [2] or Chandrayaan [3], are actively working to explore this region. Therefore, improving space situational awareness of objects in the Cislunar region is crucial to safely operating in that domain and keeping it accessible for the future.

This work outlines the LUCID spacecraft, a sub 200 kg micro-spacecraft utilising ESA's Space-Based Optical Component (SBOC) payload to observe and track objects larger than 3 metres in equivalent diameter at the mean distance of the lunar orbit.

The mission was developed using the concurrent engineering method which is further discussed in section 2. Sections 3 and 4 outline mission boundary conditions. Section 5 describes the mission's Concept of Operations (CONOPS), while Section 6 details orbit considerations. The spacecraft and its subsystems are detailed in Sections

7, 8, 9, 10, 11, 12, and 13. Section 14 presents the final system mass budget.

## 2. Concurrent Engineering

Concurrent engineering serves as a dynamic framework aiming to expedite the design process through the parallel engagement of multidisciplinary teams. This method deviates from traditional sequential or centralized design approaches, fostering interactive and iterative processes that enable real-time collaboration among experts from diverse fields (e.g. [4]). The space mission analysis context sees concurrent engineering extending across all phases of complex systems, encompassing design, development, Assembly, Integration, and Verification (AIV) activities, Launch, Ground Segment, Operations, and Disposal. ESA notably employs concurrent studies during the preliminary design phase, efficiently exploring ambitious missions within compressed timelines. Central to the success of concurrent engineering is the deployment of dedicated facilities, known as Concurrent Design Facility (CDF)s, providing collaborative environments equipped with advanced modeling tools. Additionally, a centralized system data model facilitates information sharing among experts, contributing collectively to the design process. The ESA Concurrent Engineering Workshop (CEW) in 2023 exemplified this approach, where 40 students utilized CDFs at the ESA European Space Security and Education Centre (ESEC) and Darmstadt University, employing the CDP4-COMET tool [5] to concurrently design the space and ground segments of LUCID within a one-week timeframe. This demonstration highlights the effectiveness of concurrent engineering methodologies, especially in the demanding and time-sensitive context of space mission planning and analysis.

## 3. Mission Overview

LUCID objectives and main requirements are detailed in table 1. The primary mission objective is to detect and catalogue space debris in the vicinity of the lunar orbit. In addition, the mission aims to record the objects' path to be able to define their position at a given time. The Area of Interest (AoI) lies in the cislunar region, generally defined as the volume between the Earth and the Moon. It is defined by a cone with a half-cone angle of 15°. The tip of the cone sits at Earth's center while the flat bottom sits at the lunar orbit. The cone tip is aimed at the sun while the bottom is facing the anti-sun direction.

To achieve this aim, the platform hosts the SBOC optical payload, an observation instrument designed to improve the knowledge of the distribution of space debris, which cannot be detected by ground-based sensors [6].

Furthermore, due to its large field of view, the SBOC sensor is likely to detect the same object in two consecutive images [7], resulting in a coarse orbit determination, fulfilling the above mentioned mission objectives.

The SBOC is planned to be the main payload for the ESA VISDOMS-mission (Verification of In-Situ Debris Optical Monitoring from Space) for the improvement of SSA in LEO, tracking objects less than one millimeter in diameter [8]. The LUCID mission is conceived to extend this framework, investigating objects with a diameter larger than 3 m in the cislunar environment.

Further mission drivers deal with the class and weight of the satellite, designed to be launched by a European vehicle as well as requiring a limited mass below 200 kg. The mission schedule includes the ultimate launch date, foreseen in 2030, and the commissioning phase duration, corresponding to 5 years.

ESA's new Space Debris Mitigation guidelines [9] and Space Debris Mitigation Policy [10] introduce requirements for the disposal of satellites as part of their end-of-life phase, which can either occur through atmospheric reentry (deorbiting) or an orbit transfer to a graveyard orbit. The operation shall be completed within 5 years after decommissioning and the probability of success shall be higher than 90%. To comply with these regulations, the platform design takes into account the disposal of the spacecraft once operations are concluded.

Additional details about the area of interest for debris tracking and the coverage achieved through the SBOC instrument are reported in the mission requirements (Table 1), while specifics about the payload and the observation strategy are discussed in the following section.

## 4. Optics and Sensors

### 4.1 The SBOC

The payload for this mission builds on the foundational work of the SBOC concept, a key element in the ESA Space Safety Programme [11] aimed at enhancing space situational awareness through advanced debris monitoring. Leveraging the successful demonstration of a telescope in a sun-synchronous orbit, this instrument - designed by Airbus - has been optimized to meet the specific mission objectives. This adaptation incorporates the latest advancements in space-based optical observations to improve detection accuracy and data collection efficiency. The parameters of the instrument that were used to design this mission are displayed in Table 2.

### 4.2 Design approach

The imaging strategy was designed to achieve the mission requirements for a full survey of the AoI every 24

Table 1: Initial Mission Requirements

ID	Requirement
MIS-01	The mission shall identify and catalogue objects larger than 3 meters in equivalent diameter at the mean distance of the Lunar Orbit.
MIS-02	The mission shall baseline the Space-Based Optical Component (SBOC, instrument from VISDOMS) as the primary instrument for object detection.
MIS-03	The mission shall detect objects within an area of interest (AoI) defined by: - Circular area, which normal vector lies in the Earth-Moon orbital plane - 15° half-cone-angle out of the lunar orbital plane (measured from centre of Earth) - Area is extending in the anti-Sun direction, beginning above 1000 km LEO
MIS-04	The mission shall ensure full coverage of the area of interest within 5 days.
MIS-05	The mission shall be designed to continuously cover (95% duty cycle) the AoE for 5 years.
MIS-06	The mission’s spacecraft should not exceed 200 kg of wet mass individually.
MIS-07	The mission should launch no later than 2030.
MIS-08	The mission shall utilize European launchers (Vega-C, Ariane 6).
MIS-09	The mission should follow a low-cost approach.

Table 2: Parameters of the SBOC [11].

System parameter	Working value
Aperture diameter	200 mm
Dimensions	350 mm x 450 mm x 600 mm
Power while imaging	50 W
Power in standby	5 W
Field of view	3 deg x 3 deg
Resolution	3000 px x 3000 px
Frame period	1.5 s (exposure time 0.5 s)
Baffle angle	20 deg
Daily data amount	6.336 Gigabytes

hours such that the mission would be capable of detecting 3 m objects at lunar distance. This was to be done by producing “tracklets” - 4 images taken at appropriate time intervals and stacked (see Figure 1). It was calculated that intervals of approximately 10 minutes would be sufficient to estimate debris trajectories.

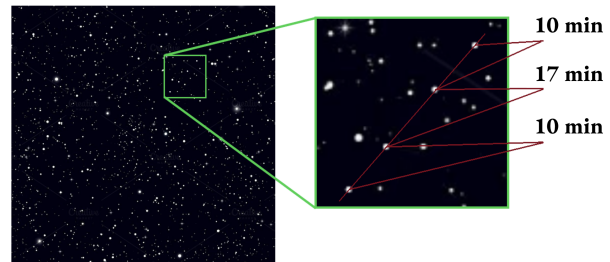


Figure 1: An example tracklet. Four stacked images create a dotted line for moving objects against a background of static stars. The spacing of the dots allows for trajectory calculation, and parallax observations enable precise determination of position and velocity of uncategorized cislunar debris.

### 4.3 Observation strategy

The AoI is divided up into 88 squares (3° x 3°) for full coverage as shown in Figure 2. To avoid atmospheric backscatter, imaging is conducted away from Earth’s surface and during eclipse when possible. The Sun-synchronous Low Earth Orbit (LEO) trajectory alternates between equinox and solstice orbits requiring different imaging cycles for each. With a 20° baffle angle, backscattering from Earth’s limb makes the AoI partially unresolvable during dawn/dusk equinox orbits (see Figure 3).

During solstice orbits, the spacecraft alternates between eclipse (optimal for anti-solar viewing) and day-

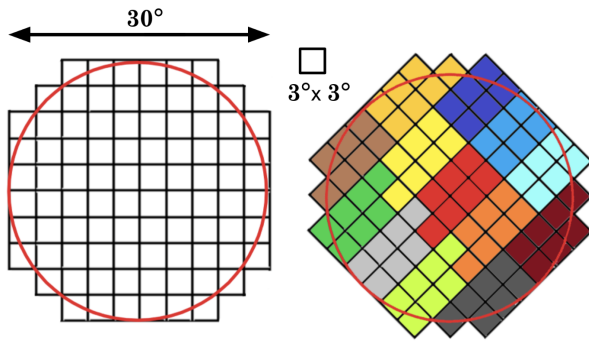


Figure 2: The 15° radius circular AoI is divided up into 88 squares (3° x 3°) for full coverage. Tracklets are mapped onto the subdivided AoI in clusters of 6 to 7 tracklets. One cluster is imaged per half-orbit.

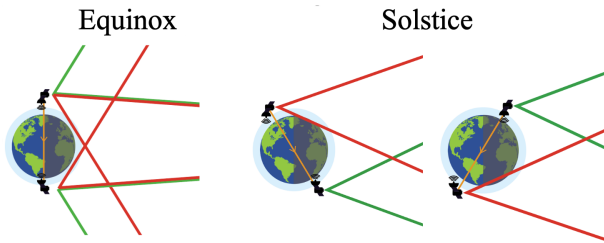


Figure 3: The two orbital modes considered in the observation strategy (not to scale). Red and green lines show obstructed and unobstructed viewing angles to the AoI, respectively.

time, where the AoI is fully obscured by the Earth. In this case, the entire AoI is imaged during the eclipse portion of the orbit in clusters of 6 to 7 tracklets. This alternating strategy ensures the entire AoI is surveyed at least once every 24 hours with minimal station keeping (Figure 4). The observation grid is rotated to 45° from north to align with the spacecraft's orbit as this reduces the number and magnitude of slewing operations required.

#### 4.4 Physical design constraints

The instrument's sensor needs protection from direct sunlight during detumbling. A single release lens cap, similar to the CHEOPS design [12], which can be opened once the orbit of the spacecraft (S/C) is stabilized, will be used.

#### 4.5 Future work

Vibration caused by reaction wheels can cause image smear. This issue was not addressed in the CEW and requires detailed analysis of the vibration modes of the S/C. Future studies should quantify this effect as it is expected

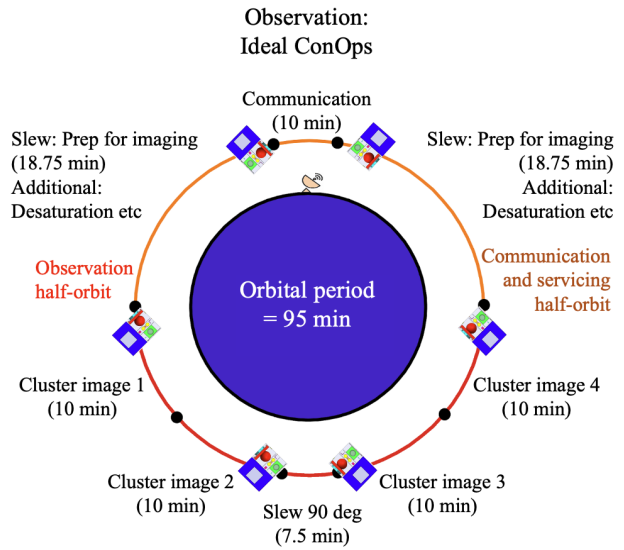


Figure 4: The spacecraft's observation and communication cycle during a 95-minute orbit, ensuring the entire AoI is imaged during the eclipse portion of solstice orbits.

to be the limiting factor on the resolving power of the instrument.

## 5. Concept of operations

The operational strategy encompasses all activities throughout the mission lifecycle and provides an estimate of the associated total costs.

### 5.1 Design Assumptions and Drivers

The development of the CONOPS incorporates decisions made by Ground Segment and Space Segment teams, as well as several key assumptions.

As an ESA mission, it is assumed that LUCID will be operated at the European Space Operations Centre (ESOC) in Darmstadt, Germany. The operational model assumes a high degree of autonomy for both the satellite and Ground Station (GS), with advanced Fault Detection, Isolation and Recovery (FDIR) automation. The MIS-05 requirement necessitates low data loss, mandating continuous monitoring of systems during satellite passes and the availability of staff for prompt response to anomalous situations.

The observational schedule serves as the primary driver of mission design, governing temporal dynamics and data collection strategies.

### 5.1.1 Mission Phases

The Launch and Early Operations Phase (LEOP) is identified as the most critical phase of the mission. During this period, operations are managed by two teams of five engineers working in complementary shifts to ensure constant monitoring. In the event of unresolved issues within a predetermined timeframe, the mission may face early termination.

The Nominal Operations phase is characterized by a high degree of automation. The orbit is equally divided into imaging and communications & service half-orbits. During the imaging half-orbit, the SBOC captures four images of the AoI in accordance with the observation strategy detailed in 4.3. The communications & service half-orbit involves spacecraft alignment for ground station communication, data transfer, and the execution of service tasks, including reaction wheel desaturation. This procedure is shown in figure 4. The spacecraft is designed to autonomously recover from minor issues and decide between continuing payload observations or downlinking science data at each pass. Abnormal situations are addressed by uploading command scripts during satellite passes, which may include preparation for collision avoidance maneuvers and software bug corrections. Ground operations during this phase primarily consist of monitoring and automated communication during satellite passes. End of Life (EoL) operations encompass passivation activities such as battery depletion, propellant tank emptying, and controlled deorbiting maneuvers, ensuring a responsible conclusion to the mission.

### 5.2 Cost Estimation

Following the definition of the CONOPS details, an estimation of the total mission costs related to Ground Operations can be formulated. These estimates are based on guidelines reported in [13] and refined through consultation with an ESA Operations Specialist. A LEOP duration of 7 days was assumed. Two models were considered, covering distinct scenarios:

Model 1 assumes the necessity for a new Operations Team for LUCID. Under this model, the estimated annual operation costs are approximately €1.5M, with the overall mission cost projected to be approximately €8M. Model 2 assumes the integration of the LUCID mission into an existing mission family at ESOC, specifically Human and Robotic Exploration. In this scenario, the estimated annual operation costs are approximately €0.8M, with the overall mission cost projected to be approximately €4.5M.

### 5.3 Future Work

Several key uncertainties require further investigation. These include the costs associated with maintaining redundant ground stations on standby, additional ground station usage requirements before and after passes, and potential emergency response team actions and associated costs. Further analysis is needed regarding the dependence on new software and whether pre-mission planning should be classified as operational rather than mission costs. The assumption that the mission can be integrated into an existing mission family may require reassessment. Additionally, the estimated one-week period for the LEOP might be excessive if no orbit transfers are required.

## 6. Trajectory Analysis

As per science requirements, the trajectory shall provide a suitable line-of-sight to the AoI without being negatively impacted by scattered sunlight from Earth's atmosphere.

Eclipses drive battery and solar panel sizing, and as these components represent significant contributors to the mass, reducing them was also a design driver. The trajectory would therefore need to have a low time spent in eclipse across the year.

The mission  $\Delta v$  should also be minimized to reduce propellant mass and the consequent tank volume. Two main contributions to the  $\Delta v$  were considered: station keeping and deorbiting/reorbiting costs, as EoL disposal is necessary to conform to space traffic management guidelines.

Finally, the spacecraft must have frequent contact with GS to downlink the significant amount of data collected during observations and to have commands up-linked to it. Selecting an orbit that allows for frequent passes of sufficient length above specified GS is necessary to reduce the amount of onboard storage required and the size and power needs of the spacecraft communication system. Making sure that the orbit allows for the use of ESA GS eventually reduces the mission costs.

### 6.1 Orbit selection

Based on the mission requirements, three families of potential orbits have been considered: LEO, Geostationary Orbit (GEO) and halo orbits around the Lagrange Point 1 of the Earth-Moon system (L1). Table 3 shows the trade-off analysis of all three orbits.

Lagrange point 1 trajectory was deemed least suitable for the purpose of this mission, mainly due high  $\Delta v$  estimates to maintain halo orbit around this unstable Lagrange point, controlled disposal and orbit insertion. A

further challenge was the relatively small distance between L1 of the Earth-Moon system to the Moon, reducing the field of view of the optical sensors.

Geostationary orbit as an equatorial orbit implies that only approximately half of the orbit would be useful for observations, with the field of view being obstructed by Earth in the other half, making geosynchronous orbit undesirable. Furthermore, the relatively high altitude of the orbit requires more powerful antennas for ground station communications.  $\Delta v$  requirements for station keeping are relatively low, but raising the orbit for end-of-life disposal on the graveyard orbit and the initial orbit insertion make up for increased mission costs.

According to the trade-off analysis, the LEO was the most suitable for the present objectives. Availability of the Sun Synchronous Orbit (SSO) allows for long observation windows with nearly constant access to sunlight, avoiding the need for primary batteries. Additionally, lower orbits are easily accessible at relatively low cost (e.g. utilising rideshares). LEO has the disadvantage of satellite experiencing air drag and therefore  $\Delta v$  for station keeping has to be accounted for but, simultaneously, controlled deorbiting of the spacecraft is much easier at the EoL. Following this trade-off analysis, the LEO family of orbits was chosen. Further details on the orbit design are described in the next subsection.

Table 3: Trade off analysis for the orbits considered.

Criterion	Weight	LEO	GEO	L1
Design Simplicity	0.20	5.0	3.0	1.0
Availability of AOI	0.30	4.0	2.0	1.0
System mass	0.10	4.0	3.0	2.0
Debris mitigation	0.15	3.0	3.0	1.0
Cost	0.25	4.0	2.0	2.0
<b>Total</b>	1.00	4.0	2.5	1.4

### 6.2 $\Delta v$ and Orbit Altitude Considerations

The spacecraft is to be deployed into a frozen SSO at an altitude that ranges from 500 km to 700 km. The Sun-synchronous orbit is designed to maintain a constant local time of the ascending node, specifically at 6 pm. This choice ensures constant illumination of the solar panels, minimizing the occurrence of eclipses, except during the winter solstice.

Drag perturbation in the SSO causes non-linear orbital decay, requiring periodic station-keeping maneuvers.  $\Delta v$  for maintenance is calculated by executing Hohmann maneuvers when the semi-major axis approaches a predefined tolerance limit, here 20km is the allowed reduction,

to place the satellite back into its intended nominal orbit. For deorbiting, two strategies are considered at this preliminary stage:

- Controlled reentry: targets a 60km perigee allowing the spacecraft to directly enter Earth’s atmosphere.
- Semi-controlled reentry: lowers the satellite’s orbit (perigee options at 150 km or 200 km) and uses atmospheric drag to gradually slow it down, causing its re-entry within a certain number of revolutions rather than instantaneously. This method minimizes the required  $\Delta v$ , making it a cost-effective approach.

Based on ESA practical experience, a  $\Delta v$  of 3 m/s has been taken into account for collision avoidance. The results of the analysis are presented in the Figure 5 below.

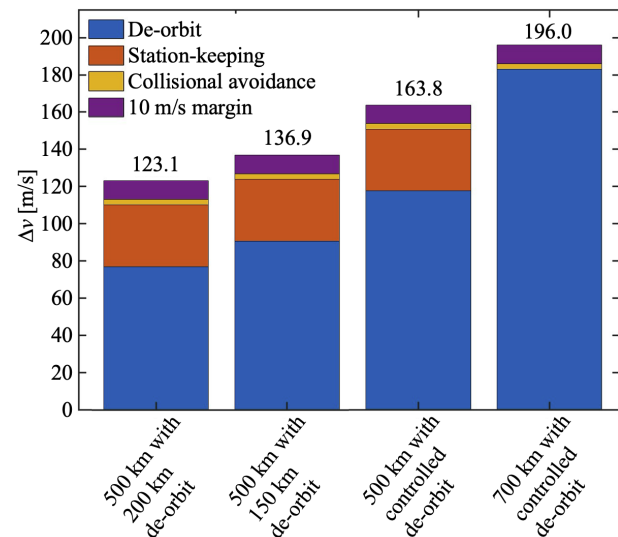


Figure 5:  $\Delta v$  requirements of different orbiting strategies.

### 6.3 Future work

Certain aspects of the orbit have been neglected at this stage of the design. Effects of the thrust being delivered within finite time, rather than instantaneously, are yet to be considered and the effects on the overall  $\Delta v$  to be analyzed. Insight into more accurate drag penalties due to solar cycles during missions should be also considered. Finally,  $\Delta v$  for inclination change to prevent Local Time at the Ascending node drift could be considered to improve accessibility for AoI and maintain desired access to solar power.

## 7. Configuration

The configuration of a spacecraft has a key role in the success of a mission, guaranteeing its integration in the

launcher, and the fulfillment of the mission objectives. Three primary drivers have been identified for the configuration subsystem: the maximum envelope, the payload fit check, and the subsystems' configuration requirements.

The maximum envelope available for the spacecraft is a direct consequence of the launcher selection. With the mission requirements of using a Vega-C launcher and keeping the cost as low as possible, Small Spacecraft Mission Service on VEGA-C launchers has been identified as the most suitable solution. According to the Vega-C user manual [14], different kinds of spacecraft with different maximum envelopes are accepted for this kind of service. For the current mission, considering a maximum wet mass of 200 kg, payload volume, and the requirement of keeping costs low, a Micro S/C has been selected for a standard launch service.

Table 4: Specifications for Mini S/C and Micro S/C class.

	Mini S/C	Micro S/C
Mass range [kg]	200-400	60-200
Max size [mm]	Ø1500 x H1800	H1200 L800 W800
CoG [mm]	XG ≤ 900	XG ≤ 450
PL Vol. [mm <sup>3</sup> ]	350x450x600	350x450x600

The payload fit check in the available envelope for the launch service offered by Vega-C is reported in Figure 6.

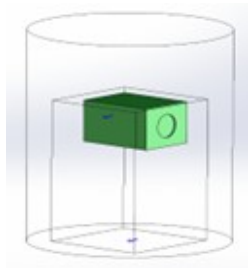


Figure 6: 3D model of the payload inside both Mini S/C and Micro S/C maximum envelope.

The last driver is related to the Configuration Requirements of the different subsystems of the spacecraft, investigated by different domain experts, defining the internal architecture for efficient functionality.

The critical and main configuration requirements that have emerged over multiple iterations of the spacecraft are:

- Power: maximization of solar array size, considering deployable solutions.
- Attitude & Orbit Control: symmetric configuration.

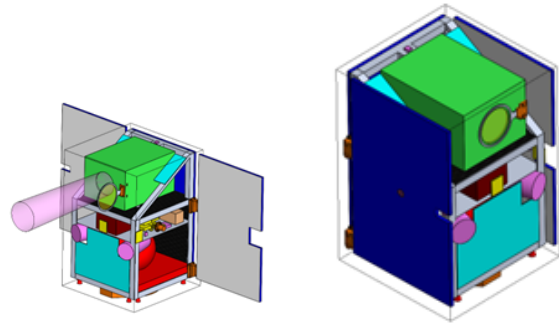


Figure 7: Last iteration 3D model of S/C. Green: Payload, Red: Propulsion, Pink: AOCS, Turquoise: Thermal, Yellow: Help please

- Thermal: facing deep space radiating elements requirements + thermal conduction paths to solar panels to decrease maximum temperatures.
- Telemetry/Telecommands: de-tumbling communication + data download → antennas facing 4 S/C planes.
- Structure: mass reduction requirements.

Once the model has converged to a final configuration, a final payload fit check in the maximum envelope available has been performed and shown in Figure 7.

### 7.1 Future work

Future studies of the mission concept could bring new pointing angles, implying new configuration requirements. Moreover, volume and mass optimization can still be performed, better exploiting the available volume, bringing to a lower mass.

## 8. Communications and Data Handling

In any space mission, the goal of the Communication and Data Handling (C&DH) subsystems is to ensure transmission of data between the spacecraft and mission control, as well as within the spacecraft itself, while managing and processing the payload data for the mission objectives. For this mission, the transmission of the 6.3 GB/day of data generated by the payload, as specified in section 4 and section 6, respectively, along with a continuous data rate of 200 kbps for telemetry and house-keeping are required. Furthermore the subsystem shall be designed to comply with International Telecommunication Union (ITU) spectrum regulations [15], reduced Direct Current (DC) power consumption, and built-in redundancy for active components.

### 8.1 System architecture

The communication system for the mission was segregated into two distinct link types. First, there is the Telemetry, Tracking and Control (TT&C) data bi-directional link, operating at S-band and utilizing a wide-beam antenna configuration. This setup ensures spacecraft coverage in any orientation. Secondly, a dedicated payload data downlink operating at X-band offers increased downlink speed to ensure the transfer of payload data.

### 8.2 Ground Segment

The GSs comprising the mission’s ground segment are chosen to maximize contact time with the mission’s orbit, with a preference for those within ESA’s core network. Due the inclination of the chosen SSO orbit, the stations are positioned as near to the northern and southern poles as possible. Specifically, the ground segment consists of ESA’s core network facility in Kiruna, Sweden and the ground station in Troll, Antarctica, operated by KSAT. For added diversity and redundancy, two additional GSs from ESA’s core network in Kourou, French Guiana, and Redu, Belgium have been incorporated.

### 8.3 Space Segment - Communications

The On-Board Computer (OBC) sends all the housekeeping data and control commands to an S-band transceiver, which modulates and forwards the data to its associated active switch. These switches direct the signal to the circulator-antenna pair best positioned towards the ground station. The same circulator-antenna pair handles reception, ensuring full-duplex operation. All necessary power splitters and combiners are in place for redundancy in active components like switches and transceivers. In contrast, payload-generated data is directed to the active X-band transmitter and is only sent to the ground segment when the satellite faces the relevant ground station and the payload remains inactive (see section 5). The schematic of the space segment is shown in Figure 8. For S- and X-band radios [16, 17] as well as the antennas [18, 19] COTS solutions are available. The resulting link shows large margins, especially for the command and telemetry link (see Table 5).

### 8.4 Space Segment - Data Handling

To achieve a power- and performance-optimised OBC, a dual-Central Processing Unit (CPU) approach, with two separate CPUs for payload data and flight data management, both based on Field Programmable Gate Array (FPGA) technology, was chosen (shown in Figure 9).

Commercial Off-The-Shelf (COTS) components [20, 21] were utilised to minimise costs while still delivering

Table 5: Communication link specifications

	S-band uplink	S-band downlink	X-band downlink
Frequency [MHz]	2067	2245	8100
Bandwidth [MHz]	0.1	0.1	20
Data rate [Mbps]	0.128	0.128	30
Bit Error Rate	$10^{-5}$	$10^{-5}$	$10^{-5}$
Link Margin [dB]	23.53	11.53	8.36

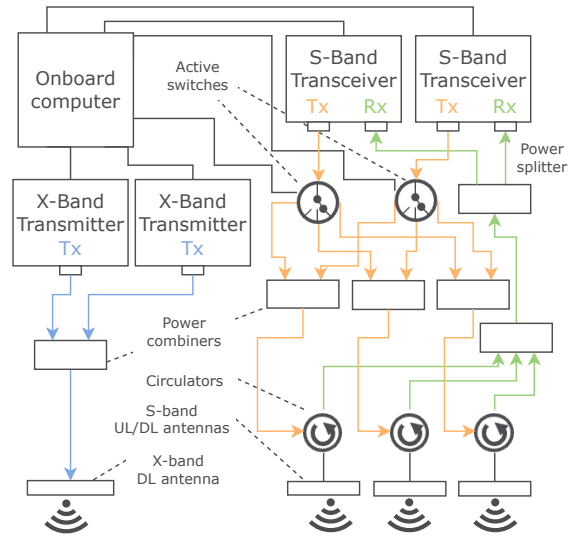


Figure 8: Communication subsystem block diagram

high performance. To deal with the vulnerability of these components to a Total Ionising Dose (TID) higher than 10 krad, an aluminium shielding was integrated. This will allow the OBC to operate reliably in the chosen SSO (see section 6) for more than five years, accumulating a TID of 8 krad at most [22].

Each processing core is equipped with a non-volatile flash-type memory for storing the flight software firmware, a volatile Synchronous Dynamic Random Access Memory (SDRAM)-type memory for program execution, and a mass storage unit for storing payload and mission data when the satellite is not in communication with the ground station. The mass memories capacity was selected to handle a maximum gap time of 40,000 seconds, determined by the trajectory specifications (see section 6). For payload data storage, we chose a 10.5 GB Solid-State Drives (SSDs) for its high performance and durability. Conversely, a 15 MB Secure Digital (SD) memory card is selected for flight data storage, favoured for its cost-effectiveness, low mass and power efficiency. Power consumption was considered in all components on board the OBC. For all three possible modes of operation

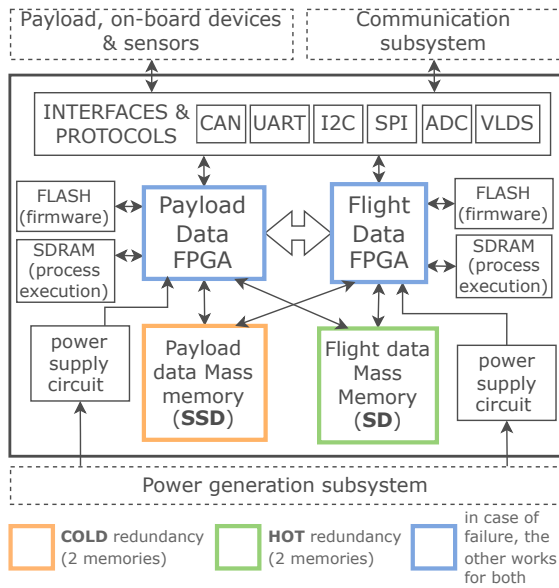


Figure 9: OBC block diagram.

indicated in section 5 (safe, normal and off), a maximum power consumption of 15W, with a 20% margin, was accounted for.

### 8.5 Future work

Future work will involve the verification of all components involved in the design. Additionally, the integration of the Communications and Data Handling Subsystem with the spacecraft structure also remains to be addressed.

## 9. Attitude and Orbital Control Subsystem

The Attitude and Orbit Control system, being a key component of the satellite, consists of reaction wheels, magnetorquers and four types of additional sensors: magnetometers, sun sensors, star trackers and GPS.

Prior to designing the Attitude and Orbital Control (AOCS), several design assumptions were driving the decision-making process. Firstly, the AOCS will control the spacecraft autonomously. The reaction wheels will be desaturated for 10% of the orbit time, one of the guidelines adopted from the CHEOPS mission [12]. Furthermore, for this stage of the design process, vibrational loads on the system were neglected. Lastly, the center of pressure was assumed to be aligned with the center of gravity. In addition to the design assumptions, several requirements were defined: the AOCS shall have a 3-axis pointing control and the sun avoidance zone is set to be the exclusion zone. A slew rate during imaging of 3 degrees per 1 minute needs to be provided to accommodate

the optical sensor requirement. Additionally, a slew rate of 160 degrees per 5 minutes during transmission needs to be administered. Eventually, a pointing accuracy of 0.001 degrees shall be maintained.

### 9.1 System sizing

With the requirements, deduced from the design of subsystems such as the payload, preliminary sizing calculations can be made. This includes the sizing of the reaction wheels and the magnetorquers. The reaction wheel sizing, for this stage of the design, relies on the required slew rate from which the torque is obtained using Equation 1.

$$T_{req} = \frac{4I_{sat}\Theta}{t^2} \quad (1)$$

Where  $T_{req}$  is the required torque (Nm),  $I_{sat}$  is the satellite's moment of inertia ( $\text{kg}\cdot\text{m}^2$ ),  $\Theta$  is the required angular displacement (rad),  $t$  is the time allocated for the maneuver (s). Magnetorquers are primarily used for desaturating reaction wheels. Reaction wheel saturation typically results from disturbance torques induced by the magnetic field, solar radiation pressure, aerodynamic forces, and the perturbational effects of oblateness on a planet's gravity. The total torque required to be compensated is  $5.021 \cdot 10^{-5}$  Nm. This torque is easily achievable with only a set of magnetorquers, thus thrusters are not needed for the reaction wheel desaturation.

### 9.2 Trade-off Analysis

Following the preliminary sizing, the preferred use of commercial-off-the-shelf components calls for a trade-off analysis. The trade-off will be performed based on chosen criteria but the following will be consistently used for all analyses:

**Mass:** with the mass budget in place, a lower mass will increase the rating of the system.

**Technology readiness level (TRL):** the time and cost allocation for this project encourages the use of high TRL systems.

**Power Consumption:** a strict power budget will favor systems with lower power consumption.

#### 9.2.1 Reaction Wheel selection

Different reaction wheels are compared and chosen based on the following criteria with a grading of 1-10 with 1 denoting the lowest and 10 the highest. A system will be graded higher for a higher maximum torque to accommodate the system sizing specifications. Similarly to the previous variable, a higher momentum storage will be graded higher.

### 9.2.2 Star Trackers

Similarly, the star trackers are compared and chosen based on the following criteria with the same grading of 1-10. Here, a higher accuracy is more favourable. Furthermore, the bigger the operating temperature range, the higher the system grade.

### 9.3 Final design

After defining the requirements and assumptions, followed by a preliminary sizing of the system, and a subsequent trade-off analysis, the final design of the AOCS will contain: Reaction Wheels providing an angular moment of 0.35 Nms with a maximum torque of 15 mNm and an accuracy of +/- 2 rpm on a power consumption of 3.432 W when on, and 2.8 W on standby, such as Aspina's ARW-200 [23]. This system shall contain four reaction wheels and one for redundancy, weighing 1 kg.

Then, magnetorquers, such as NCTR - M016 [24], with a maximum disturbance torque of  $5.021 \cdot 10^{-5}$  Nm, a magnetic moment of  $1.6 \text{ Am}^2$  running on a power consumption of 1.2 W when on, and 0.24 W on standby, and a total mass of 0.06 kg is required to meet the objective. The final design will include 4 units.

Additionally, the sensors will include 2 units of magnetometers, 6 sun sensors, 2 star trackers, and 1 GPS unit.

### 9.4 Future work

Several unresolved aspects need to be addressed for the successful realization of the project. The pointing error for the system needs to be determined, and strategies for minimizing these errors should be identified. The software components of the AOCS must be designed, including the selection of an appropriate controller. Also, electromagnetic compatibility has to be investigated.

## 10. Power

According to the current state of the art and TRL for power generation solutions, a combination of solar panels and secondary batteries has been selected for the power supply to the platform, considering conceptual operations and mission analysis. This design choice is connected to the expected lifetime requirement, to the design phase duration – according to the selected launch date – and to scientific requirements. In particular, both body-mounted and deployable solar panels are included in the design: considering the pointing requirements and the mean power budget (reported in Table 6), the sole power generated by body-mounted panels alone would not be enough. The final configuration can be seen in Figure 7.

The selected technology involves GaAs triple junction solar cells. Their reference data is reported in Table 7. Ac-

ording to the selected configuration, 375 W of power can be produced.

Secondary batteries are needed to supply power during frequent eclipses and to eventually sustain the solar arrays during peak power demand phases. Taking into account the maximum depth of discharge recommended for this class of missions, the total required capacity is equal to 500 W/h, distributed between two batteries of 250 W/h each. The suggested design includes margins and safety factors as reported in [25]: both one-string failure for solar arrays and one-cell failure for the batteries have been considered. The direct energy transfer regulation technique is employed for the solar arrays, considering sunlight partially regulated bus. As a consequence, the bus voltage is selected to be 28 V. This design choice is connected to the limited surface availability for the panels, which makes it impossible to oversize the arrays, to the simplicity of the suggested design, as well as the low budget approach.

The power conditioning and distribution unit (PCDU) is selected as an off-the-shelf component, which is generally internally redundant, according to the current and voltage requirements of the different units of the platform. Its mass and power consumption characteristics are estimated from the current market availability. After some iterations, a feasibility analysis dealing with the actual cell configuration is carried out. The results are hereafter reported: the available space makes it possible to accommodate 540 cells in the three panels, organized in 45 strings, containing 12 cells in series each. Mass values for each component of the subsystem, namely power conditioning and distribution unit, solar panels and batteries, are estimated and reported in Table 8.

### 10.1 Future work

Within the design loop of phases 0-to-B of a typical space mission development, the power budget undergoes several variations, as well as the mass and link budgets. The proposed solutions meet the purpose of a feasibility-level study (phase 0) and they need to be updated as the mission definition proceeds. As a consequence, the optimality of the solar cells accommodation may undergo some changes. Additionally, the duration of the eclipses plays an important role in the sizing of secondary batteries, and their compliance needs to be addressed once the mission analysis is consolidated.

## 11. Propulsion

The main requirement for the propulsion subsystem is to provide a  $\Delta V$  of 196 m/s for evasion maneuvers and an end-of-life deorbiting. In accordance with [25] this already includes a margin of 10 m/s. The secondary require-

Table 6: LUCID mission power budget

Subsystem	Mean Power [W]						
	OFF	INIT	CP_MANO	SCI	SLEW	COMMS	SAFE
AOCS (Attitude and Orbit Control)	0.0	27.4	40.9	40.9	40.9	40.9	40.9
COM (Communications)	0.0	16.5	13.7	17.7	17.7	45.9	23.0
INS (Instruments)	0.0	0.0	0.0	60.0	60.0	60.0	0.0
PRO (Propulsion)	0.0	23.1	14.7	23.1	23.1	23.1	23.1
PWR (Power)	0.0	2.6	2.6	2.6	2.6	2.6	2.6
TC (Thermal Control)	0.0	24.0	24.0	12.0	12.0	12.0	24.0
<b>Totals</b>	0.0	93.7	95.9	156.3	156.3	184.5	113.6
<b>Totals incl. 20% Margin</b>	0.0	112.4	115.1	187.5	187.5	221.4	136.4

Table 7: Parameters of selected solar cells

Parameter	Value
Ideal solar efficiency (BoL) [%]	29.5
Inherent Degradation Factor [-]	0.77
Active Area [%]	94.3
Cell Dimensions [mm]	80x40

Table 8: Final system mass

Component	Mass [kg] (incl. margin)
PCDU	4.4
Solar Panels	9.1
Batteries	3.6

ments are to follow a low-cost design and flight-proven hardware approach.

### 11.1 System architecture

For this mission a chemical propulsion system was chosen as it is a common choice for satellite missions of this size and orbit [26–29]. The chemical propulsion option includes different setups, with the main ones being mono- and bipropellant thrusters. Monopropellant systems are the most commonly used propulsion technology for small satellite missions. Compared to bipropellant systems, their specific impulse,  $I_{sp}$  is usually lower, which limits the amount of  $\Delta V$  that can be achieved. However they are less complex, less expensive and more reliable. For these reasons a hydrazine monopropellant system was chosen for this mission. The thrusters are fed by a pressure fed system in blowdown mode. The thruster size was set to 1 N. This is in line with heritage missions of similar size [26–29]. However to increase redundancy the number of thrusters has increased from the usual amount of

four to eight. This was possible due to the low mass of the 1N hydrazine thrusters.

### 11.2 System sizing

For the first iteration the maximum mass limit of the launcher of 200 kg was set as the wet mass. The  $I_{sp}$  of 220 S was set as a reference value considering similar projects [30]. Using Tsiolkovsky equation [13, p. 690], the fuel mass has been obtained, resulting in 17.8 kg of propellant  $m_{fuel} = 17.8$  kg (incl. 3% margin), in order to fulfil the  $\Delta V$  requirement.

To calculate the tank size, the fuel storage conditions needed to be defined. According to the thermal specifications, a tank temperature of 10°C was targeted. This is in harmony with [31] where a temperature range of 7°C to 49°C for all wet components in a hydrazine system is proposed.

The maximum operating pressure of the chosen thruster dictates the tank pressure. As an example, [30] specifies an operating pressure range from 5.5 bar to 22 bar. The pressure loss in the feeding lines to the thrusters is negligible, therefore the maximum operating pressure was also chosen as the maximum pressure of the tank.

Once the temperature and the pressure are set, the propellant density can be calculated using Coolprop [32]. This results in a fuel volume of 17.7 L.

Since this system will operate in blowdown mode it is critical to calculate the pressurant volume needed to expel the desired amount of fuel.

The pressurant gas is assumed to be an ideal gas and its expansion during thruster operation is assumed to be isentropic. This is a conservative assumption because in reality the heat loss from the expansion will be partly compensated by heat transfer from the interior of the satellite. Thus the actual tank pressure will be higher than the adiabatic case. Nitrogen was chosen over helium as a pressurant because of its lower isentropic coefficient, which sig-

nificantly reduces the required pressurant volume. In this case, the additional gas mass is compensated by the ability to use a smaller tank. Assuming all fuel is expelled a minimum tank size of 29.5 L (incl. 5% margin) is required. For the final iteration, the calculations were rerun with the actual dry mass of the satellite. This results in a fuel mass of 16.17 kg (incl. 3% margin) requiring a minimum tank volume of 26.7 L (incl. 5% margin) for blowdown operation. For this size and pressure range COTS spherical tanks are available [33, P/N:80389-1]. This results in a pressurant mass of 0.39 kg (incl. 10% margin) and a tank mass of approximately 4 kg. Using COTS thrusters with a total mass of approximately 2.5 kg the overall system mass is estimated to be 23 kg.

### 11.3 Future work

During the CEW no detailed fluid system design was performed. The introduction of filters or bends will increase pressure drop and consequently require a higher pressurant mass.

## 12. Thermal Design

The thermal design of the satellite is dictated by the platform configuration, particularly in meeting the temperature requirements of the SBOC, which must be maintained below  $-60^{\circ}\text{C}$  with a temperature stability of  $\pm 10$  mK [12]. The satellite's orbit and stabilization necessitate that the solar arrays are oriented perpendicular to the Sun. This orientation, along with the positioning of the telescope above the platform, minimizes stray light interference from both the Sun and Earth's limb, ensuring stable thermal conditions for the telescope assembly, which is exposed to deep space at approximately 4 K. The equipment must function within a specified temperature range of  $-10^{\circ}\text{C}$  to  $+40^{\circ}\text{C}$  during operational phases, and between  $-30^{\circ}\text{C}$  to  $+60^{\circ}\text{C}$  during non-operational periods. The spacecraft's thermal environment is anticipated to vary from  $+100^{\circ}\text{C}$  on the Sun-facing side to  $-80^{\circ}\text{C}$  on the opposite side [34]. Consequently, components with higher heat dissipation and more stringent operational temperature limits are strategically placed near the spacecraft's cooler regions [34].

### 12.1 Design Approach & Requirements

The thermal design strategy emphasizes the thermal isolation of the shielding from both the main platform and the telescope assembly to prevent heat transfer that could compromise the main platform's thermal stability. Due to the significant internal heat dissipation within the platform, the design addresses various operational modes, assessing whether heat must be rejected or conserved to

maintain components within their operational temperature limits. The preliminary thermal management approach utilizes passive heat transfer from warmer to cooler regions of the spacecraft, thereby reducing the need for active thermal control systems. At this stage, the thermal design is informed by heritage from previous SSO missions such as CHEOPS and PROBA-2 [35–39].

### 12.2 Final Design

The thermal management system of the platform incorporates a number of elements to ensure effective heat regulation and optimal performance. The platform is encapsulated in Multi-Layer Insulation (MLI), except in areas occupied by solar panels, radiators, and AOCs equipment.

The system includes two primary radiators, each constructed from coated aluminium sheets and measuring  $0.7 \times 1.2$  m, positioned behind the deployable solar panels. Additionally, two secondary radiators, each measuring  $0.3 \times 0.125$  m, are mounted on the SBOC. A frontal body-mounted radiator, measuring  $0.8 \times 0.8$  m, is incorporated for internal heat dissipation, featuring an aluminium silver-coated optical finish exposed through a cut-out in the MLI layer on the Carbon Fiber Reinforced Polymer panel.

Thermal coupling elements, including thermal straps and thermal switches, are employed to manage heat transfer within the platform. Thermal straps connect the SBOC radiators to the larger external radiators, facilitating efficient heat transfer. Thermal switches are integrated to selectively decouple units from radiators, thus optimizing thermal pathways under both Cold Operational Conditions (COC) operational conditions Hot Operational Conditions (HOC).

The platform is equipped with dedicated heaters for cold-sensitive components, particularly during eclipse periods and other scenarios where power dissipation is low.

To further enhance thermal control, specialised coatings and paints are applied. The aluminium radiators are coated with a silver layer, providing high reflectivity ( $\epsilon = 0.8$ ,  $\alpha = 0.25$ ). The internal walls of the platform are painted black to maximize heat absorption ( $\epsilon = 0.84$ ,  $\alpha = 0.93$ ). The combination of MLI, radiators, thermal coupling elements, heaters, and specialized coatings ensures that the platform maintains thermal stability across a range of operational scenarios.

The thermal design has a power allocation of 40 W for the COC and 48 W for the HOC. The mass allocated for the thermal control system is 6.25 kg, representing approximately 4.5% of the spacecraft's total dry mass, which aligns with the allocations in comparable missions.

### 12.3 Future Work

The radiators are sized to provide effective heat dissipation across all anticipated operational conditions. However, potential thermal interference affecting sensitive components, such as sensors, antennas, and the SBOC casing, requires full evaluation. Optimization of the power distribution and placement of heaters during eclipse periods is necessary, particularly given the substantial reduction in heat dissipation during modes such as INIT, CPMANO, and SAFE, where power dissipation can decrease to a minimum of 32 W during extended eclipses. Detailed thermal analyses will need to be conducted to address these aspects and ensure the spacecraft's thermal resilience under varying space conditions.

## 13. Structures and Mechanisms

The design of the structure revolved around the optical payload to be used to monitor debris in the cislunar environment. The concurrent design approach applied to this project had interesting impacts on the structural design methodology employed, due to the high rate of configuration variations in the early stages.

### 13.1 Design approach & requirements:

The requirements allow for a maximum spacecraft mass of 200 kg, and European launchers, therefore the decision to size LUCID according to the VEGA-C micro spacecraft specifications was made early.

The aims of the first sizing estimates were to maintain flexibility in the design to react to crucial mission achieving design needs of other sub-teams, examples of such are:

- To encase all components, hence have a structural frame equivalent to launcher fairing available space
- To provide maximum attachment surfaces inside and out, for sub-system use
- To survive the rigour of the launch environment
- To not exceed 27% of the spacecrafts dry mass, an average for LEO missions [13].

### 13.2 Initial Design Iteration:

From the design aims, points 1 & 2 showcase the safe approach to ensure that the structure did not impose any limits on sub-system design. The last two points were the key performance and optimisation indicators respectively, with surviving launch being the main design driver of the structure and minimising mass being the optimisation parameter. The structural analysis is based upon the loading

defined in the VEGA-C manual [14], as is customary for satellite designers. The axial and lateral load factors from the VEGA-C drives the design of the skeletal frame, and an analysis in the frequency domain drives the design of the sandwich panels encasing the spacecraft.

The initial structural design consisted of a homogeneous material choice - space-grade aluminium - which was driven by its good thermal properties, heritage in space, ease of machining and low cost. The skeletal frame was fitted to the VEGA-C micro package. Within exists two shelves, one acting as the optical bench providing support to the payload, the other partitioning the propulsion tank from the rest of the system. The overall structural mass of this design was 42.3 kg when including the payload launch adapter and a 5% margin for miscellaneous fixings. The resulting structure is displayed in figure 10.

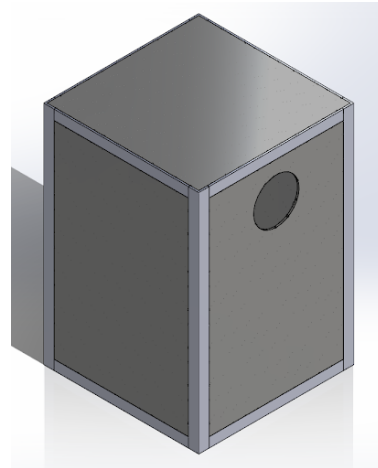


Figure 10: 1st Iteration Model of Structure

### 13.3 Trade-off analysis

At 21.2% of the overall desired wet mass, the design approach changed to drive towards lower mass. Additionally, with updated designs from across the spacecraft from other subsystems, priorities could be changed. The internal volume of the spacecraft was not fully utilised, and the payload did not need to be encased in excess structure as the thermal protection by MLI sufficiently protects the optics. As a consequence, from an initially overestimated volume of 1200 mm, 800 mm and 800 mm (height x length x width), a reduction of 100 mm in each dimension was possible. As a result, the volume of the spacecraft cuboidal section was reduced by 52.1%, and with this came a significant mass saving.

The final design can be seen in Figure 11. The trade-offs and final-phase design drivers led to a triangular support exoskeleton around the payload - this is to allow

for the fixed and deployable solar panels to still have attachment points. Additionally, titanium alloy bipods were added, to stabilise the payload and reduce vibrational effects. The final decision implemented was to replace the encasing aluminium-aluminium sandwich panels with a carbon fibre skin, saving weight at a financial penalty.

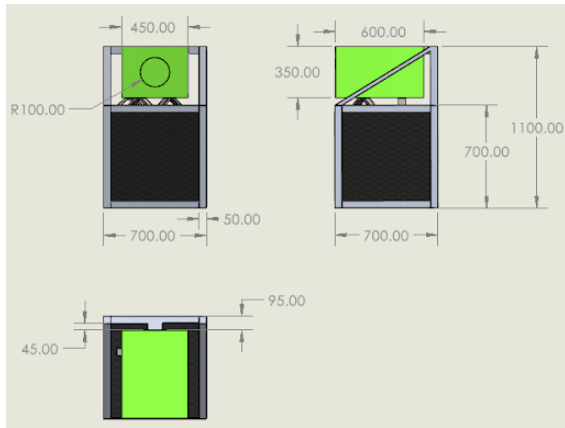


Figure 11: Engineering drawing of the final structural design with payload

#### 13.4 Final design:

The final structural arrangement of the satellite has a resemblance to that of CHEOPS [12], an ESA observation mission to characterise exoplanets, which displays a hexagonal base measuring 1.6m and a larger optical payload. Due to the desired launcher slot and the lunar focus, LUCID has a reduced volume when compared to CHEOPS: it is 27% smaller in height; as well as having half the length and width. This brings the overall weight of LUCID around 100 kg less than CHEOPS, with a final structural mass (excluding system level margin) of 27.0 kg.

Table 9: Mass breakdown of the spacecraft structure

Structural Part	Material	Mass [kg]
Skeletal Frame	Al 6061 T6	3.2
Sandwich Panels	Skin: Carbon Fibre Honeycomb: Al 5056	19.1
Shelves (e.g. battery)	Imm Aluminium	1.1
Launch Adapter	PAS 381 S	1.0
Bi-pods for Payload	Ti 6 Al 4 V	1.3
Camera Cover	Al 6061 T6	0.1
Sub-Total		<b>25.8</b>
Added Safety Margin of 5 %		1.2
Total Without System Level Margin		<b>27.0</b>

#### 14. System mass budget

Table 10: Final system mass budget

S/C Mass Budget	Margin	Mass [kg]
AOCS		8.23
Communications		8.50
Instruments		48.00
Mechanisms		2.10
Power		19.03
Propulsion		7.52
Structures		31.49
Thermal		6.25
Harness	5 %	6.56
<b>Dry Mass w/o Margin</b>		<b>137.68</b>
System Margin	20 %	27.54
<b>Dry Mass incl. Margin</b>		<b>165.22</b>
Fuel Mass		16.18
Fuel Margin	2 %	0.32
Pressurant Mass		0.36
<b>Total Wet Mass</b>		<b>182.08</b>
Launcher Adapter	5 %	2.84
<b>Total Launch Mass</b>		<b>184.92</b>

#### 15. Summary

This mission aims to observe and track objects in the vicinity of the lunar orbit using a space-based optics system to:

- Improve space situational awareness, by characterising and tracking space debris;
- Support space traffic management, which aids the safe navigation and co-ordination of spacecraft in the region;
- Contribute to scientific discoveries through detecting and studying previously unknown lunar or NEO's.

Preliminary mission and subsystem performance requirements have been set and the consequent preliminary design, unfolded in the previous sections, complies with them. Additionally, the system-level budgets (mass, power and data) follow the corresponding guidelines for the platform class. The ESA Zero Debris policy is incorporated in the mission operations and the spacecraft is flexible to launch as a co-passenger to different SSO altitudes between 500 km to 700 km.

Additional design steps for further mission development are suggested for each subsystem in order to guide potential future work related to the proposed mission.

## Acknowledgments

The students participating in the Concurrent Engineering Workshop extend their sincere gratitude to ESA's system engineers and the ESA Academy coordination Team for their support throughout the workshop and during the preparation of the IAC content. Furthermore, we deeply appreciate ESA for providing this workshop opportunity.

## References

- [1] ESA Space Debris Office, "ESA's Annual Space Environment Report," European Space Agency, Tech. Rep., 2023.
- [2] M. Smith, D. Craig, N. Herrmann, E. Mahoney, J. Krezel, N. McIntyre, and K. Goodliff, "The Artemis Program: An Overview of NASA's Activities to Return Humans to the Moon," in *2020 IEEE Aerospace Conference*, 2020.
- [3] V. Sundararajan, "Overview and technical architecture of India's Chandrayaan-2 mission to the Moon," in *2018 AIAA aerospace sciences meeting*, 2018.
- [4] M. Bandecchi, B. Melton, and F. Ongaro, "Concurrent engineering applied to space mission assessment and design," *ESA bulletin*, vol. 99, 1999.
- [5] RHEA Group, *CDP4-Comet-CE*. version 9.6.0.1, 2023.
- [6] C. Simone, "Development of an Optical Sensor Simulator for Space-Based Debris Surveillance," Master's thesis, Politecnico di Torino, 2023.
- [7] M. Michel, H. Ceeh, G. Cirillo, J. Utzmann, and S. Kraft, "Space-based optical component (sboc)," in *2<sup>nd</sup> NEO and Debris Detection Conference*, 2023.
- [8] J. Utzmann and S. Kraft, "Space-based optical component (sboc) for the esa visdoms mission," in *Proceedings of the Advanced Maui Optical and Space Surveillance (AMOS) Technologies Conference*, 2023.
- [9] ESA Space Debris Mitigation Working Group, "ESA's Space Debris Mitigation Requirements," European Space Agency, Tech. Rep., 2023.
- [10] ESA Director General's Office, "ESA's Space Debris Mitigation Policy," European Space Agency, Tech. Rep., 2023.
- [11] J. Utzmann, "Towards european space-based optical observations of debris and neos," in *Proc. 1<sup>st</sup> NEO and Debris Detection Conference, Darmstadt*. Darmstadt, Germany: ESA Space Safety Programme Office, January 2019.
- [12] R. Peyrou-Lauga and G. Bruno, "CHEOPS (Characterising ExOPlanet Satellite) thermal design and thermal analysis," in *45<sup>th</sup> International Conference on Environmental Systems*, 2015.
- [13] J. R. Wertz, D. F. Everett, and J. J. Puschell, *Space mission engineering: the new SMAD*. Space Technology Library, 2011.
- [14] ArianeSpace, *SSMS VEGA-C User's Manual, Issue*, September 2020, accessed: 2024-08-22. [Online]. Available: arianespace.com
- [15] "FCC Online Table of Frequency Allocations," Jul. 2022, accessed: September 2023. [Online]. Available: transition.fcc.gov
- [16] "SRS-4 Full-duplex High-speed S-band Transceiver," 2023, accessed: September 2023. [Online]. Available: satlab.com
- [17] "X-Band Transmitter," 2023, accessed: September 2023. [Online]. Available: endurosat.com
- [18] "S-Band Antenna Wideband," 2023, accessed: September 2023. [Online]. Available: endurosat.com
- [19] "X-Band 4x4 Patch Array," 2023, accessed: September 2023. [Online]. Available: endurosat.com
- [20] "ProASIC3E Flash Family FPGAs Datasheet," 2023, accessed: November 2023. [Online]. Available: microchip.com
- [21] "Virtex-6 Family Overview (DS150) ," 2023, accessed: November 2023. [Online]. Available: xilinx.com
- [22] G. Sebestyen, S. Fujikawa, N. Galassi, and A. Chuchra, *Downloadable Spreadsheets*. Cham: Springer International Publishing, 2018, pp. 285–286.
- [23] "ARW-2 Reaction Wheel," 2023, accessed: September 2023. [Online]. Available: satsearch.com
- [24] "Magnetorquer NCTR-M016," 2023, accessed: September 2023. [Online]. Available: SatCatalog.com
- [25] E. space agency, "Concurrent design facility studies standard margin philosophy description."

- [26] “EO-1 (Earth Observing-1) Satellite Missions Catalogue,” eoportal.org, accessed: 2023-10-30.
- [27] “SSOT (Sistema Satelital para la Observación de la Tierra) satellite missions catalogue,” eoportal.org, accessed: 2023-10-30.
- [28] eoPortal, “Demeter (detection of electromagnetic emissions transmitted from earthquake regions) satellite missions catalogue,” eoportal.org, accessed: 2023-10-30.
- [29] “VENuS (Vegetation and Environment monitoring on a New MicroSatellite) Satellite missions catalogue,” www.eoportal.org, accessed: 2023-10-30.
- [30] Ariane Group, “Heritage thruster brochure,” space-propulsion.com, accessed: 2023-09-27.
- [31] K. H. Lee, C. Y. Han, H.-K. Kim, and J. H. Moon, “Case study on thermal design improvement of hydrazine monopropellant pipelines for satellite propulsion system,” *Case Studies in Thermal Engineering*, vol. 45, 2023.
- [32] I. H. Bell, J. Wronski, S. Quoilin, and V. Lemort, “Pure and pseudo-pure fluid thermophysical property evaluation and the open-source thermophysical property library coolprop,” *Industrial & Engineering Chemistry Research*, vol. 53, no. 6, 2014.
- [33] Northrop Grumman, “Diaphragm tanks data sheets,” northropgrumman.com, accessed: 2023-09-27.
- [34] I. Melendo and R. Peyrou-Lauga, “CHEOPS Platform Thermal Architecture,” in *46<sup>th</sup> International Conference on Environmental Systems*, 2016.
- [35] W. Benz *et al.*, “The CHEOPS mission,” *Experimental Astronomy*, 2020.
- [36] M. Bergomi *et al.*, “AIV procedure for a CHEOPS demonstration model,” in *SPIE Astronomical Telescopes + Instrumentation*, 2016.
- [37] D. Magrin *et al.*, “A comparison between the opto-thermo-mechanical model and lab measurements for CHEOPS,” in *SPIE Astronomical Telescopes and Instrumentation*, 2018.
- [38] L. Blecha *et al.*, “Analytical optimization and test validation of the Sub-micron Dimensional Stability of the CHEOPS Space Telescope’s CFRP Structure,” in *Advances in Optical and Mechanical Technologies for Telescopes and Instrumentation II*, 2016.
- [39] K. Gantois *et al.*, “ESA’s second in-orbit technology demonstration mission: Proba-2,” *Bulletin 144 ESA*, 2010.